Non-stoichiometry, structural defects and properties of $LaMnO_{3+\delta}$ with high δ values ($0.11 \leqslant \delta \leqslant 0.29$)

J. A. Alonso,*[a] M. J. Martínez-Lope,[a] M. T. Casais,[a] J. L. MacManus-Driscoll,[b] P. S. I. P. N. de Silva,[c] L. F. Cohen[c] and M. T. Fernández-Díaz[d]

[a]*Instituto de Ciencia de Materiales de Madrid, C.S.I.C. Cantoblanco, E-28049 Madrid, Spain*
[b]*Department of Materials, Imperial College, London, UK SW7 2BZ*
[c]*Blackett Laboratory, Imperial College, London, UK SW7 2BZ*
[c]*Institut Laue-Langevin, B.P. 156, F-38042 Grenoble Cedex 9, France*

Strongly oxygenated $LaMnO_{3+\delta}$ perovskites, with nominal Mn^{IV} contents up to 58%, have been prepared by thermal decomposition of metal citrates followed by annealings either in air or under high oxygen pressure (200 bar). A high-resolution neutron powder diffraction study of four representative samples with $0.11 \leqslant \delta \leqslant 0.29$ reveals the presence of both La and Mn vacancies. Contrary to previous studies, it is found that there are a substantially higher proportion of Mn vacancies, depending rather sensitively on the oxidation conditions. The oxidation state for Mn calculated for the refined stoichiometry $La_{1-x}Mn_{1-y}O_3$ is in good agreement with the δ values previously determined by thermal analysis. Further to this, it is also found that as δ increases the Mn—O bond lengths shorten, the Mn—O—Mn angles progressively increase and the perovskite structure becomes more regular, which is consistent with the incorporation of Mn^{IV} cations. The presence of Mn vacancies (as much as 13% in samples prepared under high oxygen pressure) perturbs the conduction paths for the transport of holes across Mn—O—Mn, weakening the double-exchange interaction. This structural disorder explains the observed decrease of the ferromagnetic Curie temperature (T_C) as δ increases.

The structure and properties of the perovskite $LaMnO_3$ and related materials have been extensively studied in the past.[1,2] More recently, the observation of large negative magnetoresistance effects in mixed-valence manganites[3] based on $LaMnO_3$ has renewed the interest in the study of these systems. In particular, the strongly correlated magnetic and electrical properties are being widely studied. The magnetoresistance is associated with the insulator-to-metal transition which occurs in the vicinity of the Curie point, for ferromagnetic compositions such as $La_{0.7}Ca_{0.3}MnO_3$ which, thus, simultaneously exhibit metallic conductivity and ferromagnetism at low temperatures. The presence of divalent alkaline earth cations on the La sites of the perovskite induces a Mn^{III}–Mn^{IV} mixed-valence state with the formation of holes which undergo fast hopping between the two oxidation states. The temperature of both transitions depends on the Mn^{IV} content (for instance, in the $La_{1-x}Ca_xMnO_3$ system T_C varies between 182 and 278 K for Mn^{IV} contents between 14 and 38%, respectively.[4])

The parent perovskite $LaMnO_{3.00}$ (where only Mn^{III} is present) is antiferromagnetic below $T_N = 140$ K and shows a semiconducting behaviour over the whole temperature range.[5] $LaMnO_3$ crystallizes in the orthorhombic $GdFeO_3$ structural type,[6,7] with $a = 5.5392(6)$, $b = 5.6991(7)$, $c = 7.7175(9)$ Å, in the *Pbnm* setting. A strong Jahn–Teller distortion of the oxide octahedra around the d^4 Mn^{III} cations has been identified from a neutron diffraction study.[7]

A Mn^{III}–Mn^{IV} mixed-valence state can also be induced in phases of nominal stoichiometry $LaMnO_{3+\delta}$ (with Mn^{IV} content of 2δ per formula unit). These phases also show ferromagnetic behaviour for a sufficiently high content of Mn^{IV}. For instance, $LaMnO_{3.08}$ (with 16% of Mn^{IV}) was reported to be ferromagnetic with a Curie temperature $T_C = 125$ K).[5] In fact, GMR behaviour has been reported[8,9] in samples with moderate δ values, showing overall compositions $LaMnO_{3.17}$ and $LaMnO_{3.12}$.

For $LaMnO_{3+\delta}$ the oxidation of some Mn^{III} to Mn^{IV} ions reduces the driving force for Jahn–Teller distortion. Above $\delta = 0.105$ (*i.e.* 21% Mn^{IV}) there is a change in symmetry (at room temperature) from orthorhombic to rhombohedral.[10,11] In fact, the transition temperature from the orthorhombic (low-temperature form) to the rhombohedral (high-temperature form) was found to change[10] from 600 °C for $LaMnO_{3.00}$ to *ca.* −90 °C or $LaMnO_{3.15}$.

The crystal structure of the oxygen excess rhombohedral phases has been investigated by neutron diffraction.[12,13] Tofield and Scott[12] and, later on, Van Roosmalen *et al.*[13,14] concluded that instead of incorporating oxygen interstitials, as directly suggested by the formula $LaMnO_{3+\delta}$, this perovskite is defective in both La and Mn positions: for instance, a sample with a formal composition of $LaMnO_{3.158}$ was found to exhibit an actual crystallographic formula of $La_{0.95}Mn_{0.95}O_3$.

Recently[15] we have prepared $LaMnO_{3+\delta}$ phases with a wide range of δ values, $0.11 \leqslant \delta \leqslant 0.31$, by annealing finely divided precursors at moderate temperatures, either in air or under high oxygen pressure. The samples were characterized by X-ray diffraction and thermal analysis, allowing us to determine their oxygen contents (δ) very reliably. This paper complements those previous studies giving details on the actual way of incorporation of the non-stoichiometry into the crystal structures, refined from high-resolution neutron powder diffraction. Our main result is that the probability of creating equal numbers of La and Mn vacancies depends very strongly on the preparative oxidation conditions. The influence of the observed defective structure on the magnetic properties is also discussed.

Experimental

Four selected $LaMnO_{3+\delta}$ samples were prepared in polycrystalline form by a citrate technique. Stoichiometric amounts of analytical grade $La(NO_3)_3 \cdot 6H_2O$ and $Mn(NO_3)_2 \cdot 4H_2O$ were dissolved in citric acid. The metal solution was slowly evaporated and the resultant resin was subsequently decomposed at 600 °C for 12 h. A second treatment at 800 °C for 6 h enabled the total elimination of the nitrates and organic materials. The finely divided precursor powders were annealed either in air

(samples 3 and 4) or under 200 bar of oxygen pressure (samples 1 and 2), at temperatures ranging from 800 to 1100 °C. Then, the samples were slowly cooled to room temperature.

The final materials were characterized by X-ray powder diffraction (XRD) with Cu-Kα radiation. The determination of δ was performed by thermogravimetric (TG) analysis in a reducing H_2–N_2 flow, as indicated elsewhere.[15]

Neutron powder diffraction (NPD) data for $LaMnO_{3+\delta}$ were collected at room temperature in the high-resolution D2B diffractometer at the ILL, Grenoble, with a wavelength of 1.594 Å, selected from a Ge monochromator. About 5 g of each sample were contained in a cylindrical vanadium can. The time consumed in each data collection was about 3 h. The thermal evolution of samples 2, 3 and 4 was studied in the multidetector DN5 diffractometer at the Siloé reactor of the Centre d'Etudes Nucléaires, Grenoble, with a wavelength of 2.488 Å in the temperature range 2–250 K.

The Rietveld method[16] was used to refine the crystal structures, using the FULLPROF program.[17] The line shape of the diffraction peaks was generated by a pseudo-Voigt function, and the background refined to a fifth-degree polynomial. The coherent scattering lengths for La, Mn and O were, respectively, 8.24, −3.73 and 5.803 fm. In the final run the following parameters were refined: six background coefficients, zero-point, half-width, pseudo-Voigt and asymmetry parameters for the peak shape; scale factors, positional, thermal isotropic factors and unit-cell parameters. The occupancy factors of La and Mn were also allowed to vary in the last stages of the refinement. In the final cycle the shifts in the atomic parameters were zero up to the fourth decimal place.

Magnetization data were collected in an Oxford Instrument 3001 vibrating-sample magnetometer, in a remnant field of *ca.* 30 Oe, between 10 and 300 K.

Results

Structural features of $LaMnO_{3+\delta}$

The XRD patterns of samples 1–4 were characteristic of monophase perovskites with rhombohedral (samples 1–3) or orthorhombic (sample 4) symmetry, as shown in Fig. 1. Observe that there is an increase of the rhombohedral splitting of the peaks under less oxidizing conditions (*i.e.* high temperature, air). Table 1 summarizes the preparation conditions, δ values obtained by TG and unit-cell parameters determined by XRD. For samples 1 to 3 both hexagonal (a, c) and rhombohedral (a_r, α_r) descriptions of the unit cell are given.

The room-temperature NPD patterns of samples 1–3 were refined in the space group $R\bar{3}c$, hexagonal description ($Z=6$), taking as starting model that of the perovskite $LaNiO_3$, which exhibits the same symmetry.[18] La atoms are at 6a, (0,0,1/4) positions; Mn at 6b, (0,0,0); and O at 18e, (x,0,1/4). The final atomic parameters after the refinements are shown in Table 2. The good matching of the fits is illustrated in Fig. 2(*a*) for sample 3. No extra lines or additional splitting of the peaks was observed in any case. The refinement of the occupancy factor of La and Mn led to values significantly lower than 1.

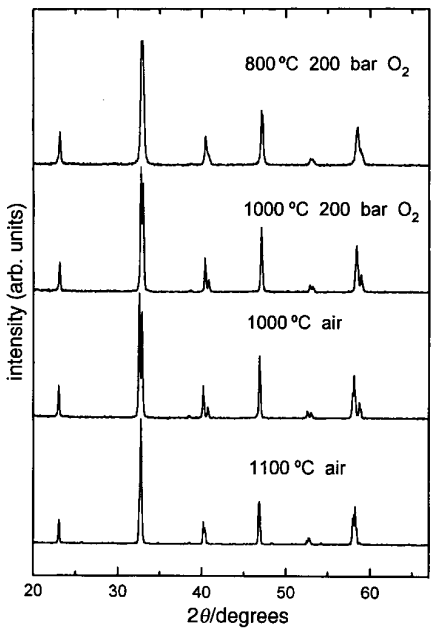

Fig. 1 XRD patterns of $LaMnO_{3+\delta}$, for samples 1 (above) to 4 (below)

Table 2 Atomic parameters for rhombohedral $LaMnO_{3+\delta}$ (samples 1–3) after the Rietveld refinement of NPD data at 295 K

sample no.	1	2	3
atom			
La B/Å^2	1.35(6)	1.38(6)	0.97(6)
f_{occ}	0.95(1)	0.97(1)	0.969(9)
Mn B/Å^2	0.3(1)	0.2(1)	0.26(10)
f_{occ}	0.89(2)	0.87(2)	0.93(2)
O x	0.4561(2)	0.4545(2)	0.4489(2)
B/Å^2	1.48(3)	1.41(3)	1.22(4)
f_{occ}	3.0	3.0	3.0
a^a/Å	5.4905(1)	5.4951(1)	5.5222(1)
b^a/Å	13.3077(1)	13.3030(1)	13.3317(1)
V/Å^3	347.42(1)	347.88(1)	352.08(1)
discrepancy factors			
R_p (%)	4.13	4.12	4.12
R_{wp} (%)	5.20	5.22	5.26
R_{exp} (%)	3.96	4.19	4.26
χ^2	1.73	1.55	1.52
R_I (%)	7.34	7.73	6.89

[a]The unit-cell parameters differ slightly from those determined from XRD (Table 1) owing to a small inaccuracy of the neutron wavelength. Note: space group $R\bar{3}c$, $Z=6$. La atoms are at 6a positions, (0,0,1/4); Mn at 6b, (0,0,0); O at 18e, (x,0,1/4).

For sample 4, the profile refinement was performed in the orthorhombic space group $Pbnm$ ($Z=4$), according to the $GdFeO_3$ structural model. La is placed at 4c, (x,y,1/4); Mn at 4b, (1/2,0,0); O(1) at 4c and O(2) at 8d, (x,y,z). Subsequently, a detailed analysis of the profile made it necessary to consider

Table 1 Preparation conditions, unit-cell parameters and volume per formula of $LaMnO_{3+\delta}$, samples 1–4, determined from XRD data. Samples 1–3 are rhombohedral, space group $R\bar{3}c$, $Z=6$; the main phase in sample 4 is orthorhombic, space group $Pbnm$, $Z=4$.

sample no.	1	2	3	4
prep. conditions	800 (200 bar O_2)	1000 °C (200 bar O_2)	1000 °C (air)	1100 °C (air)
δ(TG)	0.29	0.26	0.15	0.11
a/Å	5.4898(4)	5.4951(3)	5.5239(2)	5.54002(2)
b/Å	5.4898(4)	5.4951(3)	5.5239(2)	5.4963(2)
c/Å	13.311(1)	13.3061(8)	13.3349(7)	7.7876(4)
a_r/Å	5.453(1)	5.453(1)	5.470(1)	—
α_r/°	60.450(5)	60.509(5)	60.64(5)	—
V_f/Å^3	57.90(1)	57.99(1)	58.73(1)	59.28(1)

Table 3 Atomic parameters for sample 4 [annealed at 1100 °C(air)] after the refinement of NPD data at 295 K. The sample consists of a mixture of a main orthorhombic phase (*Pbnm*, 64.4%) and a minor rhombohedral phase ($R\bar{3}c$, 35.6%)[a]

atom		*Pbnm*	$R\bar{3}c$
La	x	0.9970(5)	
	y	0.0171(4)	
	B/Å^2	0.83(5)	0.84(8)
	f_{occ}	0.978(2)	0.978(2)
Mn	B/Å^2	0.41(7)	0.31(12)
	f_{occ}	0.946(4)	0.946(4)
O(1)	x	0.0645(5)	0.4466(4)
	y	0.4955(7)	
	B/Å^2	1.09(6)	1.06(6)
	f_{occ}	1.0	3.0
O(2)	x	0.7398(4)	
	y	0.2705(4)	
	z	0.0337(2)	
	B/Å^2	1.23(5)	
	f_{occ}	2.0	
a/Å		5.5388(2)	5.5348(1)
b/Å		5.4958(2)	5.5348(1)
c/Å		7.7843(2)	13.3438(3)
R_I		6.39	4.81

[a]Discrepancy factors: $R_p=6.32\%$, $R_{wp}=4.18\%$, $R_{exp}=2.38\%$, $\chi^2=2.18$. Note: for the orthorhomic phase: space group *Pbnm*, $Z=4$; La at 4c, (x,y,1/4); Mn at 4b, (1/2,0,0); O(1) at 4c and O(2) at 8d, (x,y,z). For the rhombohedral phase: space group $R\bar{3}c$, $Z=6$; La at 6a (0,0,1/4); Mn at 6b (0,0,0); O at 18e, (x,0,1/4).

additionally a minor rhombohedral $LaMnO_{3+\delta}$ phase (with space group $R\bar{3}c$) to correctly fit the spectra. The strong overlapping between the reflections of both polymorphs had prevented the detection of the minor rhombohedral phase prior to the Rietveld analysis of the neutron pattern. From the refined scale factors a composition of 63.6% (orthorhombic)+36.4% (rhombohedral) was determined for the mixture. The La and Mn occupancy factors were constrained for both phases. Table 3 includes the results of the refinement. Fig. 2(*b*) shows the observed and calculated NPD profiles for sample 4. Bond distances and angles are listed in Table 4. Observe that in the orthorhombic structure the MnO_6 octahedra do not show any appreciable Jahn–Teller distortion, as expected for the relatively high proportion of Mn^{IV} in the crystal (for $\delta=0.11$, $[Mn^{4+}]=22\%$), which prevents the cooperative distortion of the octahedra observed[7] in stoichiometric $LaMnO_{3.00}$.

As shown in Table 1, there is a net increase of the cell volume per formula (V_f) from 57.90 to 59.28 Å^3 as δ decreases from 0.29 (sample 1) to 0.11 (sample 4), which is consistent with the decreasing amount of Mn^{IV} cations in the structure. This is directly related to the regular variation of the Mn−O distances, quoted in Table 4. Observe that Mn−O bond lengths progressively increase from 1.9494(6) Å, for the perovskite prepared in the most oxidizing conditions, sample 1, to an average value of 1.976 Å for the orthorhombic phase present in sample 4.

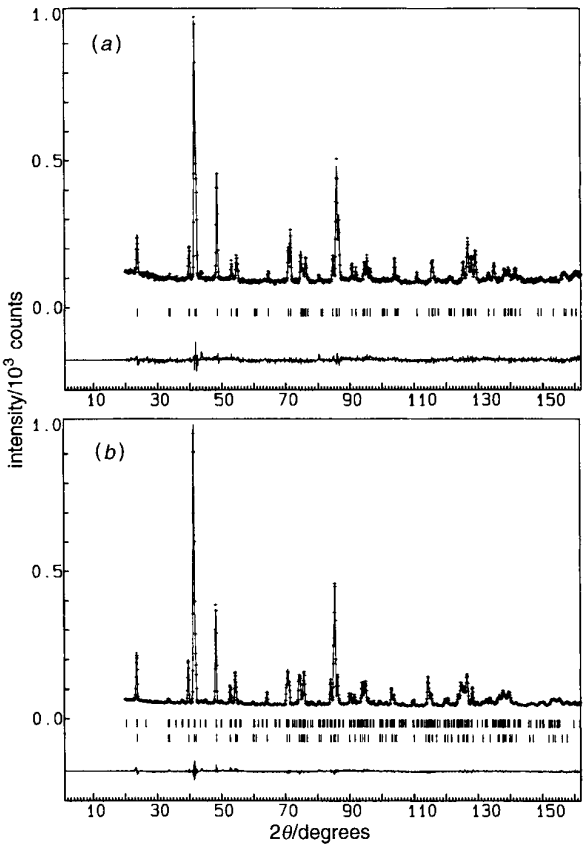

Fig. 2 Room temperature observed (crosses), calculated (solid line) and difference (at the bottom) NPD profiles for (*a*) rhombohedral $LaMnO_{3.26}$, sample 2; and (*b*) orthorhombic $LaMnO_{3.11}$, sample 4: the second series of tick marks indicate the reflections of a minor rhombohedral phase. For the sake of clarity only half of the experimental points are represented.

Some relevant parameters determined from the refinements are listed in Table 5. The crystallographic formulae of the $LaMnO_{3+\delta}$ phases, according to the refined occupancy factors for La and Mn, can be written as $La_{1-x}Mn_{1-y}O_3$, as indicated in Table 5. Under more oxidizing conditions (from sample 4 to sample 1) the amount of Mn vacancies increases more

Table 4 Selected bond distances (Å) and angles (degrees) for $LaMnO_{3+\delta}$ (samples 1–4)

sample no	1	2	3	4	
space group	$R\bar{3}c$	$R\bar{3}c$	$R\bar{3}c$	$R\bar{3}c$	*Pbnm*
Mn−O(1)	1.9494(6) ×6	1.9514(7) ×6	1.9634(6) ×6	1.969(1) ×6	1.9788(6) ×2
−O(2)	—	—	—	—	1.975(2) ×2
−O(2)	—	—	—	—	1.975(2) ×2
La−O(1)	2.504(1) ×3	2.497(1) ×3	2.479(1) ×3	2.472(1) ×3	2.891(5)
−O(1)	2.7367(5) ×6	2.7377(5) ×6	2.7492(4) ×6	2.7543(5) ×6	2.656(5)
−O(1)	—	—	—	—	2.432(4)
−O(2)	—	—	—	—	2.639(3) ×2
−O(2)	—	—	—	—	2.500(3) ×2
−O(2)	—	—	—	—	2.811(3) ×2
⟨La−O⟩	2.6591(2)	2.6576(2)	2.6591(2)	2.6602(3)	2.653(1)
O(1)−Mn−O(1)	90.84(6)	90.91(6)	91.13(5)	91.24(1)	180.0
O(2)−Mn−O(2)	—	—	—	—	91.45(17)
Mn−O(1)−Mn	165.782(7)	165.264(7)	163.477(7)	162.72(1)	159.15(5)
Mn−O(2)−Mn	—	—	—	—	162.12(9)

Table 5 Relevant parameters obtained from the structural data: crystallographic formulae, valence of Mn determined from the occupancy factors (f_{occ}), thermogravimetric data (TG) and the bond valence theory (b.v.); and tolerance factors, t

sample no.	nominal composition	actual stoichiometry	Mn valence			t^b
			f_{occ}	TG	b.v.[a]	
1	$LaMnO_{3.29}$	$La_{0.95(1)}Mn_{0.89(1)}O_3$	3.54	3.58	3.65	0.965
2	$LaMnO_{3.26}$	$La_{0.97(1)}Mn_{0.87(2)}O_3$	3.55	3.52	3.61	0.963
3	$LaMnO_{3.15}$	$La_{0.97(1)}Mn_{0.93(1)}O_3$	3.33	3.30	3.50	0.958
4	$LaMnO_{3.11}$	$La_{0.978(2)}Mn_{0.946(4)}O_3$	3.24	3.22	3.26	0.949

[a]The valence is the sum of the individual bond valences (s_i) for Mn—O bonds within the MnO_6 octahedra. Bond valences are calculated as $s_i = \exp[(r_0 - r_i)/B]$; $B = 0.37$, $r_0 = 1.760$ for the $Mn^{III}-O^{2-}$ pair, from ref. 22. Individual Mn—O distances (r_i) are taken from Table 3. [b]Tolerance factors are calculated as $t = \langle La-O \rangle / \sqrt{2} \langle Mn-O \rangle$.

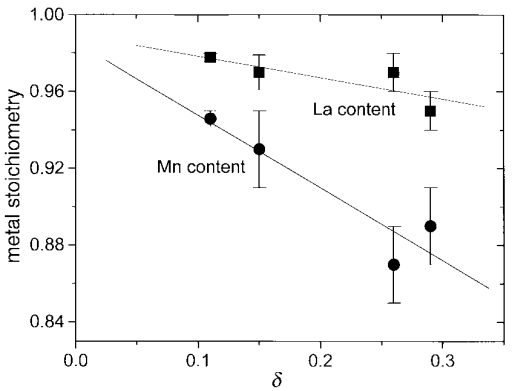

Fig. 3 Variation of the La and Mn contents with δ, determined from the neutron diffraction refinements. The full lines are guides for the eye.

quickly than the La vacancies, as shown in Fig. 3. The very oxidizing conditions (under 200 bar O_2) are more easily able to create Mn vacancies than La vacancies. The final valences for Mn calculated from the metal vacancy concentration agree quite well with those determined by thermal analysis, as shown in Table 5. The oxidative non-stoichiometry determined for these products is thus able to explain the macroscopic behaviour, represented by the δ values.

Comparing the observed Mn—O distances to the ionic radii sums[19] for a random occupancy of Mn^{III}/Mn^{IV} in the manganese positions, the observed values are systematically lower. For instance, for sample 1, $[Mn-O]_{calc} = 1.983$ Å (observed 1.949 Å, Table 4); for sample 4, orthorhombic phase, $[Mn-O]_{calc} = 2.017$ Å (observed 1.976 Å on average). This fact can be understood as an effect of the additional contraction of the lattice due to the presence of metal vacancies. For the same reason, the calculation of the valence of Mn cations within the MnO_6 coordination octahedra by means of Brown's bond valence model[20,21] systematically leads to values higher than observed (Table 5).

Comparison of low-temperature NPD and magnetization measurements

The magnetization and transport measurements have been studied for a more complete set of samples and will be described in detail elsewhere.[22] Fig. 4 shows the magnetization *vs.* temperature curves for the samples discussed in the present study. They show a ferromagnetic ordering of the Mn spins below a critical temperature. The ferromagnetic contribution to the neutron scattering is presented in Fig. 5, including the thermal evolution of the NPD patterns for sample 4. In all cases the magnetic structures can be described in terms of a single propagation vector, $\boldsymbol{k} = (0,0,0)$.[23]

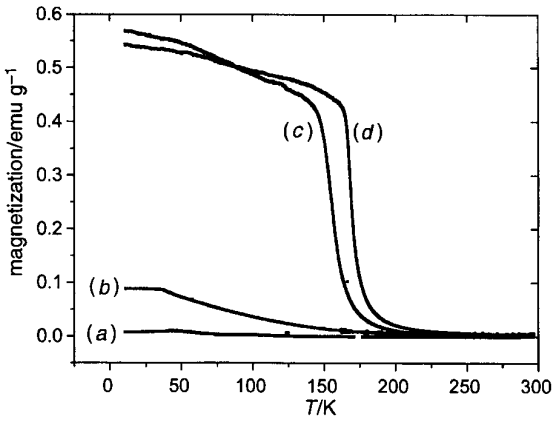

Fig. 4 Magnetization *vs.* temperature plot for $LaMnO_{3+\delta}$ ($H \approx 30$ Oe). Annealing temperature and atmosphere: (*a*) 1000 K, 200 bar O_2; (*b*) 800 K, 200 bar O_2; (*c*) 1000 K, air; (*d*) 1100 K air.

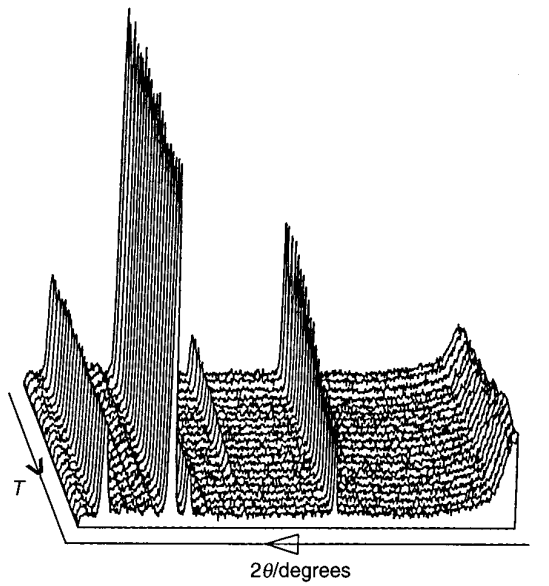

Fig. 5 Thermal evolution of the NPD patterns for $LaMnO_{3.11}$, sample 4. Below $T_C = 165$ K the magnetic contribution to the peaks of nuclear origin corresponds to the three-dimensional ferromagnetic ordering.

In Fig. 6 the Curie temperatures are plotted *vs.* δ, determined from both magnetization data and low temperature NPD experiments. Values of T_C obtained by NPD are systematically lower than those determined from the magnetization curves, as a consequence of a gradual transition from short- to long-range magnetic order, the latter taking place at temperatures about 5–15 K lower.

Discussion

In their pioneering work, Tofield and Scott[12] showed that the defect chemistry of $LaMnO_{3+\delta}$ is better described with randomly distributed La and Mn vacancies. Later on, Van Roosmalen *et al.*[13,14] concluded from a neutron diffraction experiment combined with density measurements that La and Mn vacancies are present in equal amounts in the solid, in such a way that the crystallographic formula should be written as $La_{1-x}Mn_{1-x}O_3$, with $x = \delta/(3+\delta)$. Our neutron diffraction study on samples with high δ values, prepared at relatively low temperatures from finely divided precursors, confirms the presence of significant amounts of La and Mn vacancies. Final Fourier synthesis did not yield any identifiable peaks which could suggest the presence of additional oxygen atoms in

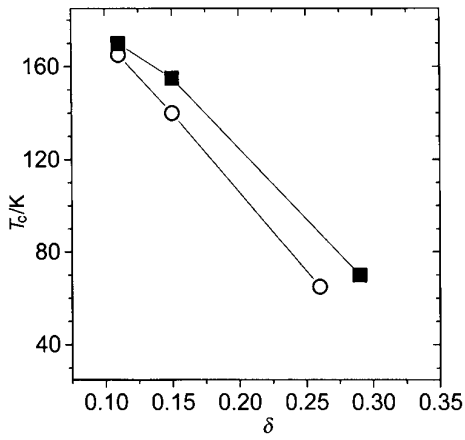

Fig. 6 Variation of the Curie temperature with δ. Full symbols from magnetization data, for samples prepared, from left to right, at 1100 K in air, 1000 K in air and 800 K in 200 bar O_2. Open symbols from NPD data, for samples prepared, from left to right, at 1100 K in air, 1000 K in air, 1000 K in 200 bar O_2 (from ref. 23).

interstitial positions, even in the more oxygenated samples. Our previous suggestion[15] that the structure of the samples prepared under oxygen pressure would probably involve oxygen interstitials, is not confirmed.

The present NPD study shows definitively that the concentrations of both kinds of metal vacancies are not equal. Moreover, the concentration of Mn vacancies increases at a higher rate when the annealing conditions of the samples become more oxidizing (*i.e.* lower temperatures and higher oxygen pressure), as shown in Fig. 3. The La and Mn vacancy concentration only become closer for low δ values, *i.e.* for samples annealed in air at higher temperatures. Note that the samples described by Tofield and Scott[12] and Van Roosmalen *et al.*[13,14] had undergone thermal treatments at even higher temperatures of 1200 or 1300 °C, respectively.

The soft-chemistry synthesis procedure described in the present work seems to favour the formation of highly defective perovskites, especially in the Mn sublattice. We show that the non-stoichiometry of $LaMnO_3$ cannot be simply denoted with a single parameter, δ or x, but requires the specification of two parameters, x and y in $La_{1-x}Mn_{1-y}O_3$. The relative values of x and y depends dramatically on the preparation procedures of the samples, in such a way that ceramic synthesis at higher temperatures favours equal values of x and y.

Our results suggest that at moderate temperatures, in the range 800–1100 °C, the higher mobility of Mn cations allows them to predominantly migrate across the perovskite structure, giving rise to a defective Mn sublattice and consequently a higher oxidation state of the remaining Mn cations. The higher mobility of Mn is probably related to the smaller size of Mn *vs.* La cations. At higher temperatures the mobility of La cations also becomes significant, giving rise to final products in which the amounts of both metal vacancies are closer.

In all cases the samples were prepared from stoichiometric mixtures of nitrates, with La : Mn = 1 : 1 ratio. The observed deviation of the 1 : 1 stoichiometry in the final perovskite phases implies the presence of minor Mn-rich phases in the products. No diffraction peaks other than those corresponding to the perovskite oxides could be detected in either the XRD or ND patterns. The segregated Mn-rich minor impurities must be present in a poorly crystallized or amorphous form, probably as a thin layer covering the surface of the perovskite crystallites.

The perovskites prepared at temperatures up to 1000 °C show rhombohedral symmetry, whereas that prepared at 1100 °C (sample 4) could be identified as a mixture with a main orthorhombic phase. This fact is consistent with the observation by Töpfer *et al.*,[11] who described an orthorhombic perovskite-type structure for $LaMnO_{3+\delta}$ at $\delta \leqslant 0.10$, while for $\delta > 0.10$ they identified a rhombohedral cell. Sample 4, with $\delta = 0.11$, is at the boundary of the phase transformation, consistent with the observed phase separation. It is worth mentioning that, in spite of the change in crystal symmetry, the determined La and Mn vacancy concentration follows the trend shown in Fig. 3 for the three pure rhombohedral compositions.

Some perovskites with oxidative non-stoichiometry have been reported to show ferromagnetic behaviour with Curie points in a comparable temperature range to those observed in the present work for the samples with lower δ values. For instance, Ranno *et al.*[24] described a T_C of 125 K for $LaMnO_{3.15}$, or $(LaMn)_{0.95}MnO_3$, whereas Töpfer *et al.*[11] obtained T_C = 171 K for $LaMnO_{3.14}$; in both cases the composition is close to that of sample 3 (also $\delta = 0.15$), with a refined stoichiometry $La_{0.97}Mn_{0.93}O_3$, and T_C (from magnetization data) of 155 K.

Fig. 6 shows that T_C decreases as δ increases, *i.e.* as the Mn^{IV} concentration increases. *A priori*, an opposite trend would be expected, since the introduction of Mn^{IV} cations (t_{2g}^3) into the $Mn^{III}O_6$ array (high-spin Mn^{III}: $t_{2g}^3e_{2g}^1$) of $LaMnO_3$ by hole doping (or as a result of deviations from the stoichiometric composition) creates empty e_g orbitals which favour the ferromagnetic double exchange. This would lead to increasing Curie temperatures with increasing δ, as demonstrated in Ca-doped manganites $La_{1-x}Ca_xMnO_3$ up to the 'optimum doping level', of 33% Mn^{IV}. In addition, for a constant doping level, T_C has been shown to increase as the tolerance factor of the perovskites is closer to 1, *i.e.* when the structure becomes more regular, with Mn—O—Mn angles closer to 180° favouring the double-exchange interactions, as shown[25] for the series $(La_{0.7-x}Y_x)Ca_{0.33}MnO_3$.

In the present case the observed trend in the variation of T_C *vs.* δ can be interpreted as a consequence of the presence of significant amounts of Mn vacancies in the structure. The final T_C value and the strength of the ferromagnetic behaviour result from an interplay between defect density, Mn^{IV} content and Mn—O—Mn bond angles. Even though the tolerance factors (Table 5) of the perovskite structures of samples 1–4 increase with δ (which is related to the progressive shortening of the Mn—O distances), the relatively high proportion of Mn vacancies (up to 13% in sample 2) perturbs the connecting paths for the holes to transport across Mn—O—Mn, and leads to weaker ferromagnetic coupling, *via* the double-exchange interaction. The presence of random vacancies may also have a strong localising effect on the available charge carriers, which reduces their mobility.[24]

Conclusions

A room-temperature, high-resolution neutron diffraction study of four selected $LaMnO_{3+\delta}$ samples with high δ values ($0.11 \leqslant \delta \leqslant 0.29$), prepared by low-temperature treatments of citrate precursors, shows highly defective perovskite structures containing both La and Mn vacancies. The Mn vacancies are present in a substantially higher proportion with respect to the La vacancies in all the samples, although the difference in the number of both kinds of defects decreases under less oxidizing conditions. (*i.e.* as δ decreases). There is a good agreement between the Mn valences determined from thermal analysis and those estimated from the defect stoichiometry $La_{1-x}Mn_{1-y}O_3$. The cell volume, Mn—O distances, Mn—O—Mn angles and tolerance factors, t, of the perovskites vary regularly with δ, *i.e.* with the oxidizing power of the materials. The high concentration of defects, mostly in the Mn sublattice, explains the anomalies observed in the magnetic properties: the samples are ferromagnetic below T_C which decreases when δ increases, even though t increases. We conclude that the preparation by soft-chemistry methods of

$LaMnO_{3+\delta}$ materials with high δ contents starting from La : Mn = 1 : 1 mixtures leads to highly Mn defective phases with anomalous magnetic properties. The synthesis of undoped La–Mn–O materials with a perfect Mn sublattice would require starting mixtures with La : Mn < 1 ratios, in such a way that the selective creation of La vacancies allows Mn cations to reach the valence corresponding to the oxidation potential given by the preparative conditions.

The authors acknowledge the financial support of the Spanish DGICyT to the project PB94–0046, and the Engineering and Physical Science Research Council of the United Kingdom.

References

1 G. H. Jonker and J. H. Van Santen, *Physica*, 1950, **16**, 337.
2 E. O. Wollan and W. C. Koeler, *Phys. Rev*., 1955, **100**, 545.
3 R. von Helmholt, J. Wecker, B. Holzapfel, L. Schultz and K. Samwer, *Phys. Rev. Lett*., 1993, **71**, 2331.
4 G. H. Rao, J. R. Sun, Y. Z. Sun, Y. L. Zhang and J. K. Liang, *J. Phys: Condens. Matter*., 1996, **8**, 5393.
5 B. C. Hauback, H. Fjellvag and N. Sakai, *J. Solid State Chem*., 1996, **124**, 43.
6 J. B. A. A. Elemans, B. Van Laar, K. R. Van der Veen and B. O. Loopstra, *J. Solid State Chem*., 1971, **3**, 238.
7 P. Norby, I. G. K. Andersen, E. K. Andersen and N. H. Andersen, *J. Solid State Chem.* 1995, **119**, 191.
8 R. Mahendiran, S. K. Tiwary, A. K. Raychadhuri, T. V. Ramakrisnan, R. Mahesh, N. Raganvittal and C. N. R. Rao, *Phys. Rev. B*, 1996, **53**, 3348.
9 C. N. R. Rao and A. K. Cheetham, *Science*, 1996, **272**, 369.
10 A. Wold and R. J. Arnott, *J. Phys. Chem. Solids*, 1959, **9**, 176.
11 J. Töpfer, J. P. Doumerc and J. C. Grenier, *J. Mater. Chem*., 1996, **6**, 1511.
12 B. C. Tofield and W. R. Scott, *J. Solid State Chem*., 1974, **10**, 183.
13 J. A. M. Van Roosmalen, E. H. P. Cordfunke, R. B. Helmholdt and H. W. Zandbergen, *J. Solid State Chem*., 1994, **110**, 100.
14 J. A. M. Van Roosmalen and E. H. P. Cordfunke, *J. Solid State Chem*., 1994, **110**, 106.
15 J. A. Alonso, M. J. Martínez-Lope and M. T. Casais, *Eur. J. Solid State Inorg. Chem*., 1996, **33**, 331.
16 H. M. Rietveld, *J. Appl. Crystallogr*., 1969, **2**, 65.
17 J. Rodríguez-Carvajal, *Physica B*, 1993, **192**, 55.
18 J. L. García-Muñoz, J. Rodríguez-Carvajal, P. Lacorre and J. B. Torrance, *Phys. Rev. B*, 1992, **46**, 4414.
19 R. D. Shannon, *Acta Crystallogr. Sect. A*, 1976, **32**, 751.
20 I. D. Brown, in *Structure and Bonding in Crystals,* ed. M. O'Keefe and A. Navrotsky, New York, 1981, vol. 2, pp. 1–30.
21 N. E. Brese and M. O'Keefe, *Acta Crystallogr. Sect. B*, 1991, **47**, 192.
22 P. S. I. P. N. de Silva, F. M. Richards, L. F. Cohen, J. A. Alonso, M. J. Martínez-Lope, M. T. Casais, T. Kodenkandath and J. L. MacManus-Driscoll, *J. Appl. Phys*., submitted.
23 J. A. Alonso, M. J. Martínez-Lope, M. T. Casais and A. Muñoz, *Solid State Commun*., 1997, **102**, 7.
24 L. Ranno, M. Viret, A. Mari, R. M. Thomas and J. M. D. Coey, *J. Phys: Condens. Matter*, 1996, **8**, L33.
25 J. Fontcuberta, B. Martínez, A. Seffar, S. Piñol, J. L. García-Muñoz and X. Obradors, *Phys. Rev. Lett*., 1996, **76**, 1122.

Paper 7/04088A; *Received* 11*th June*, 1997